



Research article

Correlation of functional magnetic resonance imaging features of primary central nervous system lymphoma with vasculogenic mimicry and reticular fibers

Huaiju Qi^{a,1}, Yu Zheng^{b,1}, Jiansheng Li^{c,*}, Kaixuan Chen^c, Li Zhou^d, Dilin Luo^c, Shan Huang^c, Jiahui Zhang^c, Yongge Lv^c, Zhu Tian^{a,**}

^a Department of Emergency, Shapingba Hospital, Chongqing University. people's hospital of Shapingba district, 400033, Chongqing, China

^b Department of Oncology, Chongqing Hospital of Traditional Chinese Medicine, 400000, Chongqing, China

^c Department of Radiology, Shenzhen Hospital of Integrated Traditional and Western Medicine, Shenzhen, Guangdong, 518104, China

^d Department of Radiology, The First Affiliated Hospital of Nanchang University, Nanchang, Jiangxi, 330006, China

ARTICLE INFO

Keywords:

Primary central nervous system lymphoma
Magnetic resonance imaging
Vasculogenic mimicry
Reticular fibers
Correlation

ABSTRACT

Objective: To deepen the imaging-pathological mechanism of primary central nervous system lymphoma (PCNSL) and provide a theoretical basis for clinical diagnosis and treatment, the functional magnetic resonance imaging (fMRI) characteristics of PCNSL were analyzed, and the relationship between the fMRI characteristics and vasculogenic mimicry (VM) and reticular fiber in PCNSL was discussed.

Methods: Ninety-six patients with PCNSL treated in our hospital were divided into three groups according to the pathological examination results, including strong positive group of VM (n = 40), weak positive group of VM (n = 56), strong positive group of reticular fiber (n = 45) and weak positive group of reticular fiber (n = 51). The levels of augmentation index and apparent diffusion coefficient (ADC) were compared among the groups. receiver operator characteristic (ROC) curve analysis was used to analyze the clinical value of ADC value in differential diagnosis of PCNSL.

Results: The levels of augmentation index in the strong positive group of VM were significantly higher than that in the weak positive group of VM, and the ADC value in the strong positive group of VM was significantly lower than that in the weak positive group of VM ($P < 0.001$). The levels of augmentation index in the strong positive group of reticular fiber were significantly higher than that in the weak positive group of reticular fiber, and ADC value in the strong positive group of reticular fiber was significantly lower than that in reticular fiber weak positive group ($P < 0.001$). Pearson correlation analysis showed that the levels of augmentation index were positively correlated with VM and reticular fiber ($r = 0.529, 0.548, P < 0.001$) and the ADC value was negatively correlated with VM and reticular fiber ($r = -0.485, -0.513, P < 0.001$). There was a significant negative correlation between necrotic lesions and VM ($r = -0.185, P < 0.05$). The area under the curve (AUC) values of average ADC value, minimum ADC value, and maximum ADC value for individual differential diagnosis of PCNSL were 0.920, 0.901, and 0.702, while the AUC

* Corresponding author. No. 3, Shajing Street, Bao'an District, Shenzhen, 518104, Guangdong, China.

** Corresponding author. No. 2 Jialang Road, Jingkou Street, Shapingba District, 400033, Chongqing, China.

E-mail addresses: lijianshengjs@21cn.com (J. Li), mhb32@sina.com (Z. Tian).

¹ Huaiju Qi and Yu Zheng contribute equally to this project.

<https://doi.org/10.1016/j.heliyon.2024.e32111>

Received 2 October 2023; Received in revised form 24 May 2024; Accepted 28 May 2024

Available online 29 May 2024

2405-8440/© 2024 The Authors. Published by Elsevier Ltd. This is an open access article under the CC BY-NC license (<http://creativecommons.org/licenses/by-nc/4.0/>).

of the combined differential diagnosis was 0.985, with a sensitivity of 95.00 % and a specificity of 92.70 %.

Conclusion: The levels of augmentation index and the ADC value of PCNSL focus are significantly correlated with VM and reticular fiber, and there is a strong negative correlation between necrotic lesions and VM. MRI imaging technology is of great significance in revealing the biological behavior of PCNSL, which can effectively reveal the relationship between VM and reticular fibers and the MRI characteristics in PCNSL, thereby providing a new imaging basis for the clinical diagnosis and treatment of PCNSL.

1. Introduction

Primary central nervous system lymphoma (PCNSL) is a relatively rare clinical neurogenic non-Hodgkin's lymphoma. Its incidence rate accounts for only 1 % of the primary intracranial tumors, and most of them are Diffuse Large B-cell Lymphoma (DLBCL) [1]. The clinical manifestations of PCNSL are closely related to the site of intracranial lymphoma invasion, and are often accompanied by changes in mental and reaction levels, which can cause symptoms such as nausea, vomiting, and headache due to increased intracranial pressure [2]. Leptomeningeal lesions can lead to headache and asymmetric cranial nerve dysfunction, and intraocular lymphoma is characterized by blurred vision and visual field defects [2]. In recent years, the incidence of PCNSL is increasing year by year, and PCNSL has the characteristics of strong tumor aggressiveness and poor prognosis [3]. Therefore, the treatment and prognosis of PCNSL have become the focus of current medical research. Some scholars have shown that about half of PCNSL patients have recurrence after treatment, and it is believed that the recurrence of tumors is related to intratumoral blood vessels [4]. Thus, the correct diagnosis of PCNSL before surgery has an important suggestive effect on the clinical treatment of patients and is of obvious help to improve the prognosis of patients. In this study, we summarized the vascular structure characteristics of a group of pathologically confirmed PCNSL, and analyzed and compared them with their magnetic resonance performance characteristics, so as to improve the understanding of the pathological mechanism of PCNSL, finally improving the level of diagnosis and differential diagnosis.

Vasculogenic mimicry (VM) is another mode of supply to tumor, in which tumor cells mimic vascular endothelial cells and form a system of tubes that are directly connected to blood vessels to transport plasma and/or red blood cells [5]. There are two forms of VM, the pattern-like matrix type and the tubular type. Among them, patterned matrix VM is composed of a PAS-positive extracellular matrix, and its main components are laminin, fibronectin, collagen IV and VI, and heparan sulfate proteoglycan [6]. This VM is distinctly different in structure and morphology from blood vessels, but it is directly connected to tumor blood vessels and can transport plasma [7]. Angiogenesis and non-angiogenic pathways in lymphoma have been shown to play an important role in tumor growth and progression, as in solid tumors, and are important for assessing patient outcomes and treatment [8]. It has been suggested that there is a close relationship between the aggressiveness of PCNSL and VM [9]. In addition, PCNSL lesions are also rich in reticular fibers, which infiltrate a large number of tumor cells, and it is believed that tumor lesions with reticular fibrous structure are highly aggressive and have a higher metastasis rate [10]. In previous studies, some scholars believe that reticular fibers are the body's defense against tumors, and there are only a small number of sparse reticular fibers or no reticular fibers around the tumor cancer nest with good differentiation and low malignancy, while rich and dense reticular fibers can be seen around the poorly differentiated and aggressive tumor cancer nest [11]. It has also been suggested that the perivascular fibrostroma is conducive to tumor invasion and dissemination [12]. Studies have found that lymphoma cells can gain greater aggressiveness and migration through interaction with reticular fibers, thereby promoting tumor spread and metastasis, and in addition, alterations in reticular fibers may also lead to the survival advantage of lymphoma cells, allowing them to continue to grow and multiply in the body [13]. The clinical symptoms of PCNSL patients are atypical. No special laboratory indicators have been found, and the common method of clinical diagnosis is imaging examination. Functional magnetic resonance imaging (fMRI) such as diffusion-weighted imaging (DWI) and perfusion-weighted imaging (PWI) have diagnostic value in PCNSL. Joshi A et al. [14] showed that advanced imaging technologies such as DWI and PWI are important in the diagnosis of PCNSL and help distinguish PCNSL from other tumors, but there are few studies on the correlation with VM and reticular fibers. MRI technology can provide images with high spatial resolution, which means that brain structures, including gray and white matter areas, can be clearly visualized [15]. The enhanced range of conventional contrast-enhanced scanning reflects the area of blood-brain barrier destruction. Conventional contrast-enhanced MRI can reflect the degree of blood-brain barrier destruction, but not the degree of tumor angiogenesis, and the application of DWI and PWI can make up for this shortcoming.

In this study, 96 patients with PCNSL treated in our hospital from January 2019 to January 2021 were picked to analyze the correlation of fMRI features of PCNSL with VM and reticular fibers. The purpose of this research was to summarize the magnetic resonance characteristics of PCNSL, analyze whether these characteristics improved the imaging diagnosis of PCNSL, and explore whether imaging can be used to roughly evaluate its biological behavior.

2. Materials and methods

2.1. General materials

A total of 156 patients with PCNSL treated in Shenzhen Hospital of Integrated Traditional and Western Medicine from January 2019 to January 2021 were selected as this study objects, and the clinical data of these patients were retrospective studied. Then, 60

patients were excluded according to the inclusion and exclusion criteria, and 96 PCNSL patients were finally included in this study. There were 61 males and 35 females, with an average age of (56.12 ± 3.56) years. Among them, there were 68 single lesions and 28 multiple lesions, with a total of 154 lesions. The largest lesion was selected for multiple lesions [16], with a total of 96 lesions. Inclusion criteria: a: After imaging examination, the diagnosis of PCNSL was confirmed by pathology; b: No prior anti-tumor therapy; c: The lesions were intracranial; d: The patient's immune function was normal; e: MRI was not preceded by hormonal therapy and chemoradiotherapy; f: Patients with systemic lymphoma were excluded upon examination. Exclusion criteria: a: Patients with other malignant tumors; b: The patient was a lactating or pregnant woman; c: Patients with important organ dysfunction; d: The patients had systemic lymphoma or lymphoma in other parts; e: Patients with congenital immunodeficiency or acquired immune impairment; f: Patients with history of hormone therapy prior to MRI; g: Patients with lymphoma elsewhere in the body. All patients were diagnosed by pathological examination to determine the VM and reticular fibers of the lesions. According to this diagnosis, the patients were divided into groups with the strong positive VM ($n = 40$), weak positive VM ($n = 56$), strong positive reticular fibers ($n = 45$), and weak positive reticular fibers ($n = 51$). There is no significant difference in age and gender among groups ($P > 0.05$). In addition, 80 patients with high-grade glioma (HGG) diagnosed in our hospital at the same time were selected as the control group to explore the clinical value of differential diagnosis of PCNSL by MRI. The operation of this experiment was approved by the Hospital Ethics Association. The selection process of general materials was shown in Fig. 1.

2.2. Outcome measures [17]

All patients were imaged with the MRI system Discovery MR750 3.0T (purchased from General Electric Company of the United States). The parameters were listed as follows: ① T1WI: 450msTR and 10msTE; ② T2WI: 4200msTR and 98msTE; ③ DWI: 7000msTR, 84msTE, B value 0 and 1 000 s/mm^2 ; ④ PWI: Glucosamine zappenate (Magnevist) was injected through forearm elbow vein high-pressure syringe. Imaging parameters: 1500mSTR, minimumTE, FOV 24128 \times 128 Matrix. ⑤ Enhanced scanning: meglumine zappenate was injected through forearm elbow vein high-pressure syringe with a dose of 0.1 mmol/kg. Imaging parameters: SET1WI 450msTR, 10msTE, 256 \times 192 Matrix. Apparent diffusion coefficient (ADC) value, T1WI, T2WI, enhanced axial lesions, and white matter MRI value of each lesion were measured with the magnetic resonance postprocessor workstation. The lesions were divided into uniform reinforcement and uneven reinforcement, and the uneven reinforcement was further divided into three regions, including high (3 points), middle (2 points), and low (1 point). The scores of different regions were calculated based on the percentage of different signal intensity zones in this level, and the sum of the regions was the lesion enhancement index. Enhancement index = (lesion enhancement value/white matter enhancement value) – (lesion non-contrast value/white matter non-contrast value), in which the enhancement index <1 was grade I enhancement, and >1 was grade II enhancement. All imaging data were determined by two senior imaging physicians, and the average value was obtained after three measurements.

Differential diagnostic value: The minimum ADC value, average ADC value, maximum ADC value and contralateral (average) ADC value of normal white matter on the opposite side of tumor parenchyma layer were measured with AW4.3 image workstation functool software. The solid areas with obvious enhancement of the tumor were selected, and the areas of the region of interest were 30–40 mm^2 . The data of each layer were sampled three times to calculate the minimum ADC value of the layer where the lesion was located.

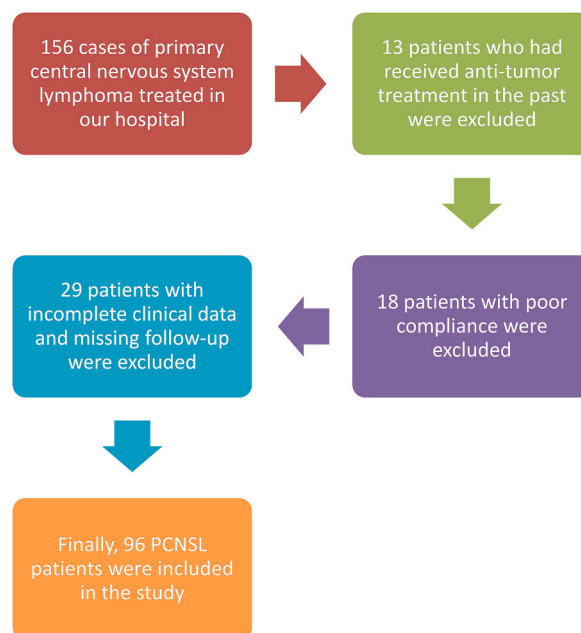


Fig. 1. The selection process of general materials of 96 patients.

The average ADC value was the final average of the maximum ADC value.

2.3. Determination of pathological results

VM [18]: The lesions presented reticular, ring, and red-striped structures. The criteria of semi-quantitative analysis: 1–2 of the 5 random visual fields showed positive manifestations of VM, and 50 % of the visual fields were positive and showed strong positive manifestations of VM, and *vice versa* were weak positive lesions.

Reticular fiber staining [19]: The presence of reticular fibers in the lesion under high magnification ($\times 400$) visual field was indicated as reticular fibers, and the presence of black stained filamentous structures was indicated as positive.

2.4. Statistical analysis

SPSS20.0 software was used to analyze the experimental data. The measurement data such as age, the augmentation index and ADC value were analyzed by Shapiro-Wilk test to determine whether the numerical variables were in accordance with the normal distribution, and the data conforming to the normal distribution were expressed as ($\bar{x} \pm s$). The independent-samples *t*-test is used to analyze whether there is a significant difference between a qualitative variable and one or more quantitative variables. The qualitative variable was a dichotomous variable in this study, so the independent-samples *t*-test was used for data between the two groups. Pearson correlation analysis was used to analyze the correlation between the characteristics and parameters of fMRI with VM and reticular fibers. The clinical value of ADC values for the differential diagnosis of PCNSL and HGG was analyzed using ROC curves. $P < 0.05$ indicated that the statistical results were statistically significant.

In order to reduce the bias, a unified input interface was designated for all survey data in this study using EpiData 3.1 software. All data were entered in double copies by two people. They entered the data on different computers and conducted consistency checks. After finding errors, the original questionnaire was checked and modified until the two databases were consistent. In addition, IBM SPSS 20.0 was used for statistical analysis. Mean and standard deviation were used to describe continuous variables, while frequency and percentage were used to describe categorical variables. Confounding bias was controlled at the analysis stage, mainly through standardization, hierarchical analysis and multivariate analysis methods, and correlation analysis.

3. Results

3.1. Comparison of the augmentation index and the ADC values in PCNSL with different VM

Compared with the weak positive VM group, the strong positive VM group had a markedly higher level in the augmentation index, and an obviously lower value in ADC ($P < 0.001$, Table 1 and Fig. 2A and B), which suggested that the existence of VM might be related to the augmentation index and the ADC values in PCNSL.

3.2. Comparison of the augmentation index and the ADC values in PCNSL with different reticular fibers

Compared with weak positive reticular fibers group, the strong positive reticular fibers group had markedly a higher level in the augmentation index, and an obviously lower value in ADC ($P < 0.001$, Table 2 and Fig. 3A and B), which further indicated that the presence of reticular fibers in tumor might be related to the augmentation index and the ADC values in PCNSL.

3.3. Correlation analysis of imaging parameters with VM and reticular fibers

Pearson correlation analysis showed that VM and reticular fibers were positively correlated with the augmentation index ($r = 0.529$ and 0.548 , respectively, $P < 0.001$) and were negatively correlated with ADC values ($r = -0.485$ and -0.513 , respectively, $P < 0.001$, Table 3), implying that the combination of VM and reticular fibers resulted in the typical delayed augmentation in PCNSL lesions.

3.4. Correlation analysis of PCNSL characteristics with VM and reticular fibers

A total of 55 lesions with iso-signal manifestation and 41 lesions with slightly low signal manifestation were found through T1WI sequence detection. High signal expression was detected in 96 lesions by DWI, and all of them with low signal by ADC. Besides, 67, 34,

Table 1
Enhancement index and ADC comparison of PCNSL with different VM ($\bar{x} \pm s$).

Groups	Cases	Augmentation index	ADC value
Strong positive VM group	40	1.14 ± 0.26	0.60 ± 0.16
Weak positive VM group	56	0.78 ± 0.19	0.85 ± 0.15
<i>t</i>		7.842	7.830
<i>P</i>		<0.001	<0.001

Note: Group *t*-test was used for comparison between groups.

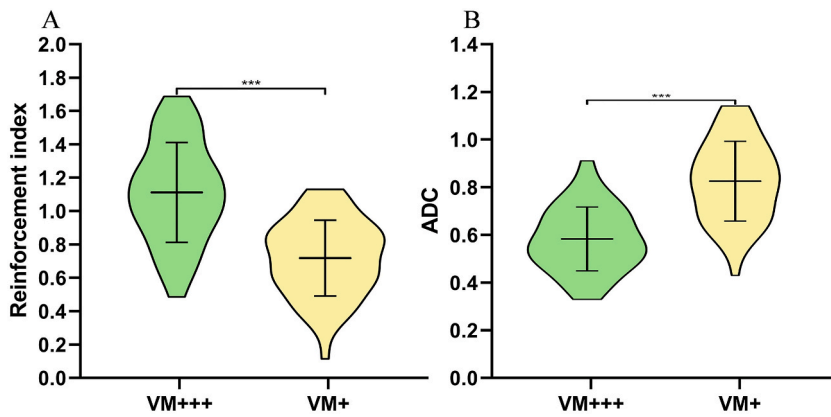


Fig. 2. Comparison of the augmentation index and ADC in PCNSL with different VM. A: Comparison of the augmentation index between the strong positive VM group and the weak positive VM group; B: Comparison of ADC values between the strong positive VM group and the weak positive VM group. Note: *** $P < 0.001$ compared between groups.

Table 2

Comparison of reinforcement index and ADC of PCNSL with different reticular fibers ($\bar{x} \pm s$).

Groups	Cases	Augmentation index	ADC value
Strong positive reticular fibers group	45	1.17 ± 0.28	0.64 ± 0.16
Weak positive reticular fibers group	51	0.82 ± 0.25	0.89 ± 0.12
<i>t</i>		6.471	8.670
<i>P</i>		<0.001	<0.001

Note: Group *t*-test was used for comparison between groups.

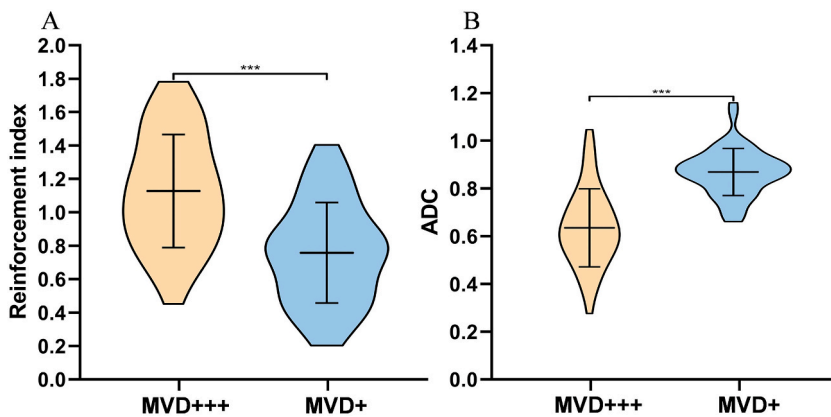


Fig. 3. Comparison of reinforcement index and ADC of PCNSL with different reticular fibers. A: Comparison of reinforcement index between the strong positive reticular fibers group and the weak positive reticular fibers group; B: Comparison of ADC values between the strong positive reticular fibers group and the weak positive reticular fibers group. Note: *** $P < 0.001$ compared between groups.

Table 3

Correlation analysis of imaging parameters with VM and reticular fibers.

Index		VM	Reticular fibers
Augmentation index	<i>r</i>	0.529	0.576
	<i>P</i>	<0.001	<0.001
ADC value	<i>r</i>	-0.485	-0.702
	<i>P</i>	<0.001	<0.001

r: Pearson correlation analysis.

28, 19, 52, and 96 lesions with lobulation, sharp corner, clenching, necrosis, meningeal infiltration, umbilical cord depression and peritumoral edema were detected, respectively. PWI showed hypoperfusion in 83 cases and iso-perfusion in 13 cases. Pearson correlation analysis showed a significant negative correlation between necrotic lesions and VM ($r = -0.185$, $P < 0.05$). Lobulation, cusp, clenching, necrosis, meningeal infiltration, umbilical cord depression and peritumoral edema had no obvious correlation with VM and reticular fibers ($P > 0.05$, Table 4), indicating that this might be related to the larger lesions selected in this study to cause cystic necrosis.

3.5. Comparison of the ADC values between PCNSL and HGG patients

The average ADC value, minimum ADC value and maximum ADC value in PCNSL group were lower than those in HGG group ($P < 0.001$, Table 5). These findings revealed the significant differences in ADC levels between PCNSL and HGG, suggesting that ADC might be of clinical significance in the differential diagnosis of PCNSL and HGG.

3.6. ROC curve analysis showed the clinical value of ADC value in differential diagnosis of PCNSL and HGG

ROC curve analysis showed that the area under the curve (AUC) of mean ADC value, minimum ADC value, and maximum ADC value for the differential diagnosis of PCNSL and HGG alone were 0.920, 0.901, and 0.702, respectively (Fig. 4A). The AUC for the combined differential diagnosis was 0.985, with a sensitivity of 95.00 % and a specificity of 92.70 %. The combined differential diagnosis value was higher (Table 6 and Fig. 4B). These results indicated that PCNSL had guiding value in MRI and could be diagnosed according to the imaging findings.

4. Discussion

PCNSL is a primary intracranial malignant tumor with a poor prognosis. The incidence of PCNSL can account for 0.3 %–1.5 % of primary tumors of the intracranial central system, and the supratentorial deep white matter is the most common site [20]. Due to the changes in the vascular permeability of PCNSL, a large number of reticular fibrous tissues and VM appear, so it is highly aggressive and metastasis, and the recurrence rate of patients after treatment is high, which not only greatly increases the pain of patients, but also brings a part of the medical burden to the society and family [21,22]. Therefore, how to effectively evaluate the severity of PCNSL and predict the recurrence risk of PCNSL have become the focus of the current medical research.

At present, MRI is an important examination method for clinical diagnosis of PCNSL and evaluation of cranial space-occupying lesions, which can be used as a screening method due to its high resolution and multi-sequence imaging of soft tissues, as well as low cost [23]. PCNSL pretends to occur in the deep supratentorial white matter and grows infiltratively around the perivascular space [4]. In this experiment, the T1WI sequence showed equal and slightly low signal detection lesions, and the T2WI sequence showed equal signal and high intensity, indicating that necrosis, cystic change and edema lesions were more likely to occur, and the standing effect was obvious. DWI is an imaging technique that evaluates tissue structure by non-invasive detection of the diffusion movement of water molecules in tissues, and the high signal expression of DWI and the low signal expression of ADC often indicate that the tumor tissue cells are tightly structured, with abundant reticular fibers, small extracellular space and low water content [24,25]. PWI can be used to effectively evaluate the peripheral hemodynamic changes of body lesions. PWI is based on the analysis of the contrast medium first passing through the capillary bed. When the contrast medium passes through the tested tissue for the first time, the contrast medium is mainly distributed in the capillary bed, causing a change in the uniformity of the local microscopic magnetic field and resulting in a decrease in T2 signal. The rCBV value calculated from the area under the T2 time-signal curve can reflect the tissue blood volume and reflect the degree of angiogenesis [26]. In this experiment, the lesions detected by DWI were all hyperintense, the lesions detected by ADC were all hypointense, and the manifestations of PWI lesions were equal and hypoperfusion, which could help to

Table 4
Correlation analysis of PCNSL characteristics with VM and reticular fibers.

Indicators		VM	Reticular fibers
Lobulation	<i>r</i>	0.125	0.136
	<i>P</i>	0.539	0.516
Sharp corner	<i>r</i>	-0.078	-0.035
	<i>P</i>	0.128	0.884
Clenching	<i>r</i>	0.125	-0.158
	<i>P</i>	0.362	0.891
Necrosis	<i>r</i>	-0.185	-0.151
	<i>P</i>	0.016	0.523
Meningeal infiltration	<i>r</i>	-0.056	-0.024
	<i>P</i>	0.058	0.912
Umbilical cord depression	<i>r</i>	0.128	0.045
	<i>P</i>	0.716	0.815
Peritumoral edema	<i>r</i>	0.268	-0.007
	<i>P</i>	0.241	0.715

r: Pearson correlation analysis.

Table 5
Comparison of ADC values between PCNSL and HGG patients ($\bar{x} \pm s$).

Groups	Cases	Mean ADC value	Minimum ADC value	Maximum ADC value	Contralateral ADC value
PCNSL group	96	0.78 ± 0.12	0.57 ± 0.10	1.12 ± 0.30	0.85 ± 0.11
HGG group	80	1.05 ± 0.16	0.80 ± 0.15	1.32 ± 0.22	0.84 ± 0.05
<i>t</i>		12.778	12.135	4.954	0.751
<i>P</i>		<0.001	<0.001	<0.001	0.454

Note: Group *t*-test was used for comparison between groups.

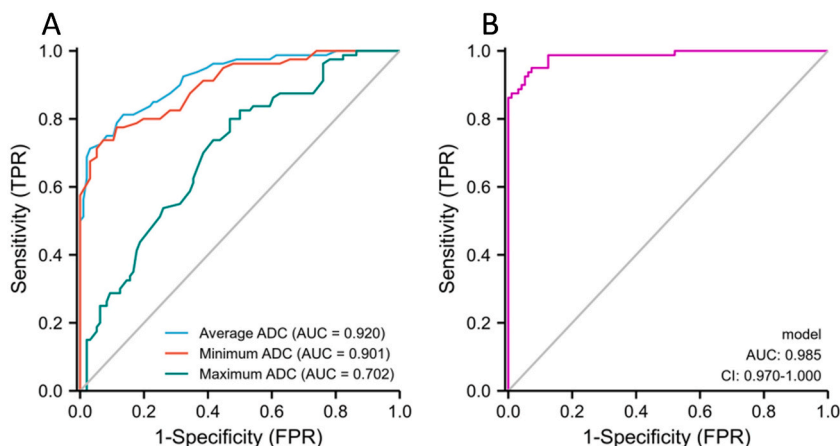


Fig. 4. ROC curve analysis of ADC value in differential diagnosis of PCNSL and HGG. A: Diagnostic value of single index, including mean ADC value, minimum ADC value, maximum ADC value; B: Value of combined differential diagnosis of mean ADC value, minimum ADC value, maximum ADC value.

Table 6
ROC curve analysis of ADC value in differential diagnosis of PCNSL and HGG.

Indicators	AUC	95%CI	Sensitivity	Specificity	Cut-off value	<i>P</i>
Mean ADC value	0.920	0.881–0.959	71.30	96.90	0.965	<0.001
Minimum ADC value	0.901	0.856–0.946	73.80	92.70	0.705	<0.001
Maximum ADC value	0.702	0.625–0.778	80.00	53.10	1.145	<0.001
Combined differential diagnosis	0.985	0.970–1.000	95.00	92.70	–	<0.001

Note: AUC: area under the ROC curve; 95%CI: 95 % confidence interval; Cut-off Value: indicates the critical value.

diagnose PCNSL, in consistent with the results of Xia W et al. [27]. The high intensity of DWI showed that the destruction of the blood-brain barrier was greater than that of the dense area of tumor cells. At the same time, due to the fact that intracranial primary B-cell lymphoma and its tendency to grow along the vascular gap, the degree of damage to the blood-brain barrier around the blood vessels was significant, and the contrast agent was easy to leak into the corresponding area, resulting in significant enhancement, in consistent with the results of this study [28]. The previous study has found that the common features of lymphoma include lobulation, umbilical fovea and sharp angle, and umbilical fovea is closely related to tumor cell growth and angiogenesis [29]. Lobulation, sharp angle, fist clenching, necrosis, meningeal infiltration, umbilical fovea, and peritumoral edema were also detected in this experiment, among which lobulation and peritumoral edema were the most common.

At present, there are no studies that directly prove the relationship between PCNSL and angiogenic mimicry and reticular fibers. However, the early study has suggested that the high aggressiveness and recurrence rate of PCNSL are related to VM and reticular fibers in tumor tissues. The structure of VM is significantly different from that of blood vessels, which has the effect of providing nutrients to tumor tissues and providing important help for the growth and metastasis of tumor cells. Among them, the strong positives on pathological examination were mostly rich pattern-like matrix VM, and the weak positives were mostly scattered pattern-like matrix VM [8,30,31]. During imaging, richly patterned stromal VM significantly increases intercellular contrast media, thereby increasing tumor intensification [32]. In this experiment, the augmentation index level of the strong positive VM group was significantly higher than that of the weak positive VM group, and the ADC value was significantly lower than that of the weak positive VM group. It was suggested that Tumor tissue cells with rich pattern-like stromal VM structures were compact and more prone to metastasis. Although PCNSL is an aggressive tumor, tumor cells infiltrate and destroy the blood vessel wall, and the mechanism of vascular edema is formed by perivascular exudation, which result in a significant decrease in the osmotic pressure of peritumoral blood vessels, and the diffusion of water molecules is not limited, leading to a significant increase in ADC value [33]. The study has shown that the minimum ADC

value of tumor can more accurately reflect the internal biological characteristics and malignancy of tumor tissue, which has become a "hot spot" in tumor differential diagnosis research in recent years [34]. The augmentation index level of the strong positive VM group was higher, and the in-depth analysis may be due to the fact that the contrast medium could enter with the plasma and diffuse through the tumor space, so that the contrast medium in the gap increased, thereby enhancing the tumor strengthening. It has been found that the change of the augmentation index of glioma MRI is consistent with the change of tumor microvessel density, which may become an important imaging index for preoperative evaluation of tumor biological characteristics, and has guiding value for the selection and evaluation of tumor treatment [35]. At the same time, PCNSL is surrounded by abundant reticular fibers, which are mostly ring-shaped and radial. The reticular fibers provide scaffolds for the growth of tumor cells, on the one hand, support the growth of tumor cells, and on the other hand, play a protective role, which is conducive to tumor invasion and invasion [36]. In this experiment, the level of the augmentation index in the reticular fiber strong positive group was significantly increased, and the ADC value was significantly decreased. It was suggested that reticular fiber tissue could prevent the entry and exclusion of contrast media. The more reticular fiber structures were, the higher the delayed enhancement level was. At the same time, a large number of reticular fibers led to the decrease of extracellular space and water content of tumor cells, and the ADC value would also decrease accordingly. This study speculated that tumor cells around blood vessels obtained nutrition supply by infiltrating and destroying blood vessel walls to leak out nutrients, while tumor cells far from blood vessels transported oxygen and nutrients through VM to meet growth needs, which might be the main reason why PCNSL lacking blood supply had less necrosis and light necrosis degree [37]. PCNSL cells are tightly arranged, the extracellular space is small, the blood vessels are few, and the large number of reticular fibers makes the contrast medium spread and clear slowly, which is another important factor contributing to the delayed enhancement of tumor performance [38]. Thus, this study speculated that the destruction of the blood-brain barrier, VM and intratumoral reticular fibers together led to the "slow in and slow out" of the contrast agent in PCNSL lesions and the typical delayed reinforcement. Some scholars believe that reticular fibers are the body's defense against tumors. There are only a small number of sparse reticular fibers around the tumor cancer nest with good differentiation and low malignancy, or no reticular fibers. In contrast, poorly differentiated and aggressive tumor nests can be surrounded by abundant, dense reticular fibers [39]. It has also been suggested that the perivascular fibrostroma favors tumor invasion and dissemination [40]. Therefore, we speculate that the reticular fibers distributed around the PCNSL blood vessels are conducive to the formation of a "sleeve-like" infiltrating structure of the tumor, which can cause extensive destruction of the blood vessels of PCNSL tumors and is highly aggressive.

Pearson correlation analysis showed that VM and reticular fibers were positively correlated with the augmentation index and were negatively correlated with the ADC values. Besides, a negative correlation existed between necrotic lesions and VM. The analysis might be due to the necrotic lesions, and the MRI appearance of ADC values was negatively correlated with VM. Due to the small number of blood vessels in PCNSL, the limited nutrients leaked from the broken vessel walls, resulting in necrosis. This is explained by the presence of VM, which are connected to blood vessels and increase the blood supply to the tumor, thereby meeting the oxygen and nutrients needed for tumor growth [41]. The augmentation index was positively correlated with VM and reticular fibers. Given the late time point of MRI enhancement scan, all PCNSLs showed delayed augmentation. However, fibrous tissue can delay strengthening because it can block the entry and discharge of contrast medium, so the more reticular fibers, the more obvious the delayed reinforcement. The results of this study further indicated that there was a strong correlation between imaging features and structural changes of PCNSL, which could be used as an important means to diagnose PCNSL and evaluate its aggressiveness, providing help to guide the treatment plan. PCNSL is a rare intracranial tumor with strong aggressiveness and poor prognosis, and the clinical treatment is mainly based on chemotherapy combined with corticosteroids. HGG has a high degree of malignancy, and treatment is mainly surgery. PCNSL and HGG are both infiltrative-growing tumors, and tumor cells can infiltrate and grow periphery. Moreover, there is a case-crossover situation under the influence of conventional MRI, which is difficult to distinguish, but the treatment methods are completely different. Early identification of PCNSL and HGG, as well as the targeted treatment can help improve the quality of life and prognosis. Some scholars compared the differences between ADC and conventional MRI parameters between PCNSL and HGG groups. The results showed that the values of ADC_{min} and ADC_{total} in the PCNSL group were lower than those in the HGG group. Also, it was found that the diagnostic accuracy of distinguishing PCNSL from atypical HGG showed $AUC = 0.927$ (95 % confidence interval CI 0.735–0.959) through ROC curve analysis, which suggested that conventional MRI features combined with ADC values could further improve the ability to distinguish between PCNSL and HGG [42]. In the present study, the AUC of the combined average, minimum and maximum ADC values in the diagnosis of PCNSL was 0.985. It could be seen that different ADC parameters of tumor parenchyma could provide a molecular imaging basis for the differentiation of PCNSL and HGG, which was a safe, non-invasive and convenient imaging method. The MRI findings of PCNSL are suggestive for the clinical diagnosis and treatment. Improving the understanding of PCNSL and mastering its characteristic imaging manifestations can help early diagnosis, early treatment, and improve the survival rate of patients. MRI imaging technology has high promotion value in the diagnosis of lymphoma, which can provide accurate diagnosis basis for clinical treatment, reduce medical costs, and improve the quality of life of patients. With the continuous development and improvement of MRI imaging technology, its application prospect in the field of lymphoma diagnosis will be broader.

In general, there was a significant correlation between PCNSL lesion augmentation index as well as ADC value and VM as well as reticular fibers. Also, there is a strong negative correlation between necrotic lesions and VM. MRI imaging technology is of great significance in revealing the biological behavior of PCNSL, which can effectively reveal the relationship between VM and reticular fibers and magnetic resonance imaging characteristics in PCNSL, providing a new imaging basis for the clinical diagnosis and treatment of primary central nervous system lymphoma.

Research strengths: The lack of blood vessels, the presence of VM structure, and the abundance of reticular fibers in PCNSL are the main factors leading to low early enhancement and obvious enhancement in the delayed phase, and these factors are also related to peritumoral edema and focal necrosis. This study will improve the understanding of the imaging mechanism of PCNSL, so as to identify

meaningful imaging features and improve the imaging diagnosis of PCNSL.

Limitations: However, due to the short duration of this experiment, no physiological, anatomical, and morphological measurements (before, during and after treatments) have been performed to confirm their findings. In addition, the sample size is small and the observation indicators are limited, and the results may be biased. Moreover, the patients included in this study are only patients from our hospital, which may affect the generalizability of the study results. In the future, the sample size and study design need to be further expanded and the study design needs to be refined to validate the results of this study. In addition, the augmentation and necrosis characteristics of PCNSL were significantly related to tumor neovascularization and mature blood vessels. However, the small number of blood vessels in PCNSL does not fully explain these features of PCNSL, and the internal blood oxygen supply and imaging manifestations of PCNSL still need to be further verified by DWI and PWI examinations.

Funding

No funding was received for this paper.

Data availability statement

The datasets used and/or analyzed during the current study are available from the corresponding author upon reasonable request.

Ethics approval and consent to participate

All procedures performed in studies involving human participants were in accordance with the ethical standards of the institutional and/or national research committee and with the 1964 Helsinki declaration and its later amendments or comparable ethical standards.

The study was approved by the Ethics Committee of The Shenzhen Hospital of Integrated Traditional and Western Medicine (2019-SZH-004).

Patient consent for publication

Written Informed consent was obtained from all individual participants included in the study. The patients participating in the study all agree to publish the research results.

CRedit authorship contribution statement

Huaiju Qi: Writing – original draft, Investigation, Formal analysis. **Yu Zheng:** Software, Resources, Methodology, Investigation. **Jiansheng Li:** Project administration, Formal analysis, Data curation, Conceptualization. **Kaixuan Chen:** Methodology, Investigation. **Li Zhou:** Software, Resources. **Dilin Luo:** Validation, Supervision, Data curation. **Shan Huang:** Supervision, Resources. **Jiahui Zhang:** Supervision, Resources, Methodology. **Yongge Lv:** Methodology, Data curation. **Zhu Tian:** Writing – review & editing, Methodology, Formal analysis.

Declaration of competing interest

The authors declare that they have no known competing financial interests or personal relationships that could have appeared to influence the work reported in this paper.

Acknowledgments

Not applicable.

References

- [1] T.T. Batchelor, Primary central nervous system lymphoma: a curable disease, *Hematol. Oncol.* 37 (Suppl 1) (2019) 15–18.
- [2] Primary central nervous system lymphoma, *Nat. Rev. Dis. Prim.* 9 (1) (2023) 30.
- [3] Y. Narita, et al., Phase I/II study of tirabrutinib, a second-generation Bruton's tyrosine kinase inhibitor, in relapsed/refractory primary central nervous system lymphoma, *Neuro Oncol.* 23 (1) (2021) 122–133.
- [4] Y. Ota, [Primary central nervous system lymphoma: essentials of imaging findings], *Brain Nerve* 73 (10) (2021) 1079–1086.
- [5] A.J. Maniotis, et al., Vascular channel formation by human melanoma cells in vivo and in vitro: vasculogenic mimicry, *Am. J. Pathol.* 155 (3) (1999) 739–752.
- [6] J.L. Ma, et al., Role of Twist in vasculogenic mimicry formation in hypoxic hepatocellular carcinoma cells in vitro, *Biochem. Biophys. Res. Commun.* 408 (4) (2011) 686–691.
- [7] G. Morales-Guadarrama, et al., Vasculogenic mimicry in breast cancer: clinical relevance and drivers, *Cells* 10 (7) (2021) 1758.
- [8] D. Ribatti, et al., Vascular growth in lymphomas: angiogenesis and alternative ways, *Cancers* 15 (12) (2023) 3262.
- [9] Y. Yue, et al., Vasculogenic mimicry in head and neck tumors: a narrative review, *Transl. Cancer Res.* 10 (6) (2021) 3044–3052.
- [10] M. Norrington, et al., Neuroinflammation preceding primary central nervous system lymphoma (PCNSL) - case reports and literature review, *J. Clin. Neurosci.* 89 (2021) 381–388.
- [11] T. Ushiki, Collagen fibers, reticular fibers and elastic fibers. A comprehensive understanding from a morphological viewpoint, *Arch. Histol. Cytol.* 65 (2) (2002) 109–126.

- [12] J.W. Pollard, Macrophages define the invasive microenvironment in breast cancer, *J. Leukoc. Biol.* 84 (3) (2008) 623–630.
- [13] A.Y. Lin, et al., Discovering the fibroblastic reticular cell in the immune tumor microenvironment in lymphoma, *J. Clin. Invest.* 133 (13) (2023) e171310.
- [14] A. Joshi, et al., Primary CNS lymphoma in immunocompetent patients: appearances on conventional and advanced imaging with review of literature, *J. Radiol. Case Rep.* 16 (7) (2022) 1–17.
- [15] S. Schob, et al., Diffusion-weighted MRI reflects proliferative activity in primary CNS lymphoma, *PLoS One* 11 (8) (2016) e0161386.
- [16] X. Lin, et al., Atypical radiological findings of primary central nervous system lymphoma, *Neuroradiology* 62 (6) (2020) 669–676.
- [17] M. Kim, et al., Impact of lesion size on reproducibility of quantitative measurement and radiomic features in vessel wall MRI, *Eur. Radiol.* 33 (3) (2023) 2195–2206.
- [18] R. Folberg, et al., Vasculogenic mimicry and tumor angiogenesis, *Am. J. Pathol.* 156 (2) (2000) 361–381.
- [19] Y. Sugita, et al., Endoglin (CD 105) is expressed on endothelial cells in the primary central nervous system lymphomas and correlates with survival, *J. Neuro Oncol.* 82 (3) (2007) 249–256.
- [20] K. David, et al., Primary central nervous system lymphoma: treatment and nursing management of immunocompetent patients, *Clin. J. Oncol. Nurs.* 25 (4) (2021) 439–448.
- [21] P. Mondello, et al., Primary central nervous system lymphoma: novel precision therapies, *Crit. Rev. Oncol. Hematol.* 141 (2019) 139–145.
- [22] D. Chihara, et al., Primary central nervous system lymphoma: evolving biologic insights and recent therapeutic advances, *Clin. Lymphoma, Myeloma & Leukemia* 21 (2) (2021) 73–79.
- [23] R.F. Barajas, et al., Consensus recommendations for MRI and PET imaging of primary central nervous system lymphoma: guideline statement from the International Primary CNS Lymphoma Collaborative Group (IPCG), *Neuro Oncol.* 23 (7) (2021) 1056–1071.
- [24] X. Lu, et al., Diagnostic performance of DWI for differentiating primary central nervous system lymphoma from glioblastoma: a systematic review and meta-analysis, *Neurol. Sci.* 40 (5) (2019) 947–956.
- [25] W. Xia, et al., Multiparametric-MRI-based radiomics model for differentiating primary central nervous system lymphoma from glioblastoma: development and cross-vendor validation, *J. Magn. Reson. Imag.* 53 (1) (2021) 242–250.
- [26] E. Scola, et al., Assessment of brain tumors by magnetic resonance dynamic susceptibility contrast perfusion-weighted imaging and computed tomography perfusion: a comparison study, *Radiol. Med.* 127 (6) (2022) 664–672.
- [27] W. Xia, et al., Deep learning for automatic differential diagnosis of primary central nervous system lymphoma and glioblastoma: multi-parametric magnetic resonance imaging based convolutional neural network model, *J. Magn. Reson. Imag.* 54 (3) (2021) 880–887.
- [28] J. Liang, et al., Application of IVIM-DWI in detecting the tumor vasculogenic mimicry under antiangiogenesis combined with oxaliplatin treatment, *Front. Oncol.* 10 (2020) 1376.
- [29] C.H. Suh, et al., MRI as a diagnostic biomarker for differentiating primary central nervous system lymphoma from glioblastoma: a systematic review and meta-analysis, *J. Magn. Reson. Imag.* 50 (2) (2019) 560–572.
- [30] K. Qiao, et al., RNA m6A methylation promotes the formation of vasculogenic mimicry in hepatocellular carcinoma via Hippo pathway, *Angiogenesis* 24 (1) (2021) 83–96.
- [31] J. Li, et al., Inhibitory effects of B-cell lymphoma 2 on the vasculogenic mimicry of hypoxic human glioma cells, *Exp. Ther. Med.* 9 (3) (2015) 977–981.
- [32] A.K. Herrera-Vargas, et al., Pro-angiogenic activity and vasculogenic mimicry in the tumor microenvironment by leptin in cancer, *Cytokine Growth Factor Rev.* 62 (2021) 23–41.
- [33] F. Eisenhut, et al., Classification of primary cerebral lymphoma and glioblastoma featuring dynamic susceptibility contrast and apparent diffusion coefficient, *Brain Sci.* 10 (11) (2020) 886.
- [34] R. Mulyadi, et al., The role of pretherapeutic diffusion-weighted MR imaging derived apparent diffusion coefficient in predicting clinical outcomes in immunocompetent patients with primary CNS lymphoma: a systematic review and meta-analysis, *Asian Pac. J. Cancer Prev. APJCP* 23 (7) (2022) 2449–2457.
- [35] G. Shukla, et al., Advanced magnetic resonance imaging in glioblastoma: a review, *Chin. Clin. Oncol.* 6 (4) (2017) 40.
- [36] J.E.C. Bromberg, et al., The role of rituximab in primary central nervous system lymphoma, *Curr. Oncol. Rep.* 22 (8) (2020) 78.
- [37] B. Nico, et al., Aquaporin-4 expression in primary human central nervous system lymphomas correlates with tumour cell proliferation and phenotypic heterogeneity of the vessel wall, *Eur. J. Cancer* 48 (5) (2012) 772–781.
- [38] D. Liu, et al., Delayed contrast enhancement in magnetic resonance imaging and vascular morphology of primary diffuse large B-cell lymphoma (DLBCL) of the central nervous system (CNS): a retrospective study, *Med. Sci. Mon. Int. Med. J. Exp. Clin. Res.* 25 (2019) 3321–3328.
- [39] X. Hu, et al., Reticular fibre structure in the differential diagnosis of parathyroid neoplasms, *Diagn. Pathol.* 18 (1) (2023) 79.
- [40] M. Lütge, et al., Differentiation and activation of fibroblastic reticular cells, *Immunol. Rev.* 302 (1) (2021) 32–46.
- [41] H.S. Tang, et al., Angiogenesis, vasculogenesis, and vasculogenic mimicry in ovarian cancer, *Int. J. Gynecol. Cancer* 19 (4) (2009) 605–610.
- [42] Y.X. He, et al., Conventional MR and DW imaging findings of cerebellar primary CNS lymphoma: comparison with high-grade glioma, *Sci. Rep.* 10 (1) (2020) 10007.